

# Evidence for Accretion: High-Resolution X-ray Spectroscopy of the Classical T Tauri Star TW Hydrae

Joel H. Kastner

Chester F. Carlson Center for Imaging Science, Rochester Institute of Technology, 54 Lomb  
Memorial Dr., Rochester, NY 14623; jhk@cis.rit.edu

David P. Huenemoerder, Norbert S. Schulz, Claude R. Canizares  
MIT Center for Space Research, 70 Vassar St., Cambridge, MA, 02139, U.S.A.  
and

David A. Weintraub

Dept. of Physics and Astronomy, Vanderbilt University, Nashville, TN, 37235, U.S.A.

## ABSTRACT

We present high resolution X-ray spectra of the X-ray bright classical T Tauri star, TW Hydrae, covering the wavelength range of 1.5-25 Å. The differential emission measure derived from fluxes of temperature-sensitive emission lines shows a plasma with a sharply peaked temperature distribution, peaking at  $\log T = 6.5$ . Abundance anomalies are apparent, with iron very deficient relative to oxygen, while neon is enhanced relative to oxygen. Density-sensitive line ratios of Ne IX and O VII indicate densities near  $\log n_e = 13$ . A flare with rapid ( $\sim 1$  ks) rise time was detected during our 48 ksec observation; however, based on analysis of the emission-line spectrum during quiescent and flaring states, the derived plasma parameters do not appear strongly time-dependent. The inferred plasma temperature distribution and densities are consistent with a model in which the bulk of the X-ray emission from TW Hya is generated via mass accretion from its circumstellar disk. Assuming accretion powers the X-ray emission, our results for  $\log n_e$  suggest an accretion rate of  $\sim 10^{-8} M_{\odot} \text{ yr}^{-1}$ .

*Subject headings:* stars: Xrays — stars: T Tauri: individual (TW Hya) — stars: formation — stars: disks

## 1. Introduction

Over the past two decades — beginning with *Einstein* and continuing through the most recent observations by the *Chandra X-ray Observatory* and the X-ray Multi-Mirror Mission

(XMM) — X-ray observatories have produced an increasingly detailed and comprehensive census of X-ray sources in star formation regions. These observations have firmly established the presence of strong X-ray emission as one of the defining characteristics of stellar youth (Feigelson & Montmerle 1999). Moreover, high-energy emission from young stars is central to many, seemingly disparate aspects of star and planet formation, from the chemical evolution of dark clouds to formation of chondrules found in meteoritic inclusions.

Despite considerable recent progress, astronomers are still grappling with a fundamental understanding of the physical mechanisms that lead to X-ray emission from regions of young stars. For deeply convective T Tauri stars (TTS), coronal activity due to intense surface magnetic fields has long been proposed as the source of the X-rays (Feigelson & Montmerle 1999 and references therein). A coronal origin appears plausible for weak-lined T Tauri stars (wTTS), if the hypothesis is correct that these stars have either lost or become decoupled from their circumstellar accretion disks and generally are rotating more rapidly than the disk-enshrouded classical T Tauri Stars (cTTS). Coronal activity may not be the only possible source of X-rays, however. There is reason on theoretical grounds to expect X-ray emission from star-disk interactions (e.g., Shu et al. 1997). Such interactions likely persist at least through the cTTS evolutionary stage.

Existing X-ray data are inconclusive as to the relation of TTS coronae to the coronae of main sequence and evolved stars, and to the potential distinctions between X-ray emission from coronae vs. from star-disk interactions (e.g., Feigelson 2001). Moderate resolution ( $R \sim 50$ ) CCD X-ray spectroscopy by *ASCA* provides tantalizing evidence for abundance anomalies in the X-ray spectra of TTS (e.g., Skinner et al. 1997; Skinner & Walter 1998) that are similar to those seen in *ASCA* CCD spectroscopy of active, evolved stars (e.g., White 1996). These same studies also make clear, however, the limitations of stellar X-ray spectroscopy with CCDs. The High Energy Transmission Gratings Spectrometer (HETGS) on *Chandra* now provides a much more powerful tool for the study of X-ray emission from stars (Canizares et al. 2000). With a resolution of  $\sim 1000$ , *Chandra*/HETGS can easily resolve individual spectral lines and line complexes, providing an arsenal of greatly improved plasma diagnostics (e.g., Drake et al. 2001).

The TW Hydrae Association (TWA; Kastner et al. 1997, Webb et al. 1999, Zuckerman et al. 2001) holds great potential for spectral studies of X-ray emission from TTS. Due to the proximity of the association ( $D \sim 50$  pc) and the lack of intervening, ambient cloud material, the X-ray flux of a *typical* TWA star ( $F_x \sim 3 \times 10^{-12}$  erg cm $^{-2}$  s $^{-1}$ ) rivals or exceeds that of the most X-ray luminous TTS in dark clouds (Kastner et al. 1997). As the X-ray spectra of TWA stars can be obtained free of contamination from absorbing dark cloud material, any line-of-sight absorption can be attributed almost entirely to circumstellar gas.

To date, the only TWA star that has been studied in detail at X-ray wavelengths is TW Hya itself (Kastner et al. 1999). At a distance of only 57 pc from Earth (Wichmann et al. 1998), TW Hya is the nearest known classical TTS, and is one of the best studied examples of a young star-disk system; its dust-rich, gaseous accretion disk evidently is viewed nearly face-on (Kastner et al. 1997; Krist et al. 2000; Wilner et al. 2000; Weintraub, Kastner & Bary 2000; Trilling et al. 2001). Based on ASCA and ROSAT spectral data, the X-ray emission from TW Hya was modeled by Kastner et al. as arising in a two-component plasma with  $T_{x,1} \simeq 2$  MK and  $T_{x,2} \simeq 10$  MK. The emission evidently is attenuated by a variable absorbing column, with  $N_H$  ranging from  $\sim 5 \times 10^{20}$  cm $^{-2}$  to  $\sim 3 \times 10^{21}$  cm $^{-2}$ . From this modeling, Kastner et al. (1999) concluded that the strong emission from TW Hya at  $\sim 1$  keV (Fig. 1, top) probably was dominated by lines of highly ionized Fe.

Here, we present high-resolution Chandra/HETGS spectroscopy of TW Hya. These data dramatically confirm that the X-ray emission from TW Hya is dominated by emission lines — although Fe emission is surprisingly weak and Ne emission surprisingly strong. Furthermore, Chandra/HETGS spectra call into question a coronal origin for the X-ray emission from TW Hya.

## 2. Observations and Results

TW Hya was observed with Chandra/HETGS for 48 ks in June, 2000 (observation identifier 5) in the default configuration (timed exposure, ACIS-S detector array), under nominal operating conditions. Data were re-processed with CIAO software to apply updated calibration, and events were cleaned of the detector artifacts on CCD 8 (“streaks”). Spectral responses were made with CIAO (Chandra Interactive Analysis of Observations) software. Lines were measured with ISIS<sup>1</sup> (Houck & DeNicola 2000), and emission measure and abundances were modeled with custom IDL software. More detailed descriptions of the processing can be found in Huenemoerder, Canizares, & Schulz (2001), in which the same techniques were applied to HETGS spectra of II Pegasi.

The resulting Chandra/HETGS spectrum yielded 3700 first order medium energy grating (MEG) counts, and 1080 first order high energy grating (HEG) counts. We present the TW Hya spectrum in Fig. 1 (bottom). The Chandra/HETGS data confirm that the X-ray spectrum of TW Hya longward of  $\sim 10$  Å ( $E < 1.2$  eV) is dominated by emission lines. The measured flux (0.45–6.0 keV) is  $3.7 \times 10^{-12}$  ergs cm $^{-2}$  s $^{-1}$  ( $2.5 \times 10^{-3}$  photons cm $^{-2}$  s $^{-1}$ ), corresponding to  $L_x = 1.4 \times 10^{30}$  ergs s $^{-1}$  at the distance to TW Hya ( $D = 57$  pc). Because

---

<sup>1</sup>ISIS is available from <http://space.mit.edu/CXC/ISIS>

the HETGS response matrix is nearly diagonal, this flux result is obtained independent of a model spectrum.

The Chandra/HETGS spectrum demonstrates that the  $\sim 1$  keV region of the spectrum is dominated by lines of *highly ionized Ne* — not Fe (Fig. 2). Furthermore, lines of ionized Fe are conspicuous for their absence across much of the HETGS spectral regime; instead, besides Ne, the most prominent lines are due to O, Mg, and Si (Table 1).

About 30 ks into the observation, a flare occurred during which the flux doubled in about 1 ks. The flux immediately began a rather linear decay, followed by a possible minor flare (Fig. 3). We inspected lightcurves in narrower bands and in lines for indications of similar variability. Harder bands had greater modulation, and the flare is apparent in some lines (Ne x 12 Å), but not others (O VIII 19 Å).

### 3. Modeling

We have performed a variable abundance, differential emission measure (DEM) analysis on line fluxes or upper limits (for details, see Huenemoerder et al. 2001 and references therein). The DEM is defined as  $n_e^2(T)dV(T, n_e)/dT$ , and is a measure of the density-weighted plasma volume as a function of temperature and density. It is, in a sense, the only emergent property derivable from the integrated line fluxes without imposition of a physical model, other than the assumptions required to validate the emissivity model. In our fit to the fluxes, we allowed abundances to be free parameters, but omitted density sensitive lines and used a low-density emissivity database. This database (the Astrophysical Plasma Emission Database, or “APED”; Smith et al. 2001) tabulates emissivities versus temperature and density for a plasma in collisional ionization equilibrium (“CIE”). CIE implies a stable ionization state of a thermal plasma under the *coronal approximation*, in which the dominant processes are collisional excitation and ionization from the ground state, and radiative and dielectronic recombination.

Model results described below (§§ 3.1, 3.2) were derived from analysis of the entire observation (i.e., combined quiescent and flaring time intervals). We also divided the observation into pre-flare and flare intervals and measured the line strengths in each partition. To increase the potential significance of a temperature diagnostic, we also summed the Ne IX fluxes and compared to the summed Ne x flux. In neither the individual lines nor in the summed cases do we find any significant differences (larger than one standard deviation) between quiescent and flare states. In particular, while the elevated high-energy continuum suggests a modest increase in the contribution of high- $T_x$  material to the DEM during the

flare, we find that ratios of the brightest temperature- and density-sensitive lines did not vary significantly during the course of the observation (Fig. 4). We also find no measurable changes in abundances between quiescent and flare states. Hence, for further analysis, we only considered the entire observation, in order to derive the physical conditions of the mean state of TW Hya.

### 3.1. Emission Measure Distribution and Abundances

The emission measure distribution derived from fitting the Chandra/HETGS spectrum of TW Hya displays a sharp peak at  $\log T_x = 6.5$  (Fig. 5). The peak at  $\log T_x \simeq 7.7$  represents an upper limit and reflects the absence of lines of highly ionized Fe from the spectrum. The integrated volume emission measure lies within the range  $1.3 - 1.7 \times 10^{53} \text{ cm}^{-3}$ . The results are the same, to within the uncertainties, during both quiescent and elevated X-ray emission time intervals. The DEM model fitting suggests the fractional abundances (relative to solar) of O, Ne, and Fe are 0.3, 2.0, and 0.2, respectively, while abundances of N, Si, and Mg are roughly solar. The accuracies of these derived abundances are about 20%, as determined from ad hoc perturbations of the model.

Fig. 2 shows a model spectrum predicted from this “best-fit” DEM model, convolved with the instrument response, overlaid on the observed spectrum. Qualitative agreement of continuum and many lines is good; density-sensitive features are discrepant, as expected, since the fit includes only temperature-sensitive lines and is based on low-density emissivities.

### 3.2. Densities

The lack of [O VII] emission at 22.1 Å in the spectrum of TW Hya (and the consequent small ratio of the intensity of this line to that of the 21.8 Å line) implies large electron densities of  $n_e \geq 10^{12} \text{ cm}^{-3}$  for the emitting region of this cTTS. The He-like Ne IX triplet at 13.45, 13.55, and 13.7 Å provides an even more stringent density constraint of  $\log n_e = 12.75$  (cgs;  $2\sigma$  limits 12.6–13.0), assuming CIE. We caution that these results are predicated on the assumption that the EUV continuum from TW Hya is not driving the He-like lines to their high-density ratios (an intense EUV radiation field can depopulate the metastable level, thereby weakening the forbidden line and enhancing the intercombination line; e.g., Porquet & Dubau 2000). This assumption appears justified, however, as the UV continuum of TW Hya is relatively weak (though it does exhibit bright UV line emission; Costa et al. 2000).

The Mg XI He-like triplet is also density sensitive. However, the 9.0-9.5 Å region shows

a curious lack of observed Mg features, relative to the model. There are several possible explanations: the derived abundance could be too high (although this is unlikely, given the strength of Mg XII 8.42 Å); higher-level Lyman transitions of Ne X that are absent from the APED tables may be present in the Mg XI region; and/or the model may underestimate the mass of plasma at high temperatures ( $\log T_x \geq 7.0$ ) due to the lack of lines that are diagnostic of this temperature regime.

## 4. Discussion

### 4.1. TW Hya and active, late-type stars: similarities and differences

In certain respects, the Chandra/HETGS spectrum of TW Hya is similar to that of active, late-type, main sequence or post-main sequence stars, for which the abundances of Fe also appear depleted, and the abundances of Ne appear enhanced, with respect to solar (e.g., HR 1099, Drake et al. 2001; II Peg, Huenemoerder et al. 2001). Fig. 6 compares Chandra/HETGS spectra of TW Hya and such (primarily) RS CVn systems in the 13.3 Å to 15.4 Å region, which encompasses the Ne IX triplet and several prominent lines of highly ionized Fe. For the RS CVn binaries the X-ray emission presumably arises in magnetically confined, coronal plasma. It is apparent from this Figure that the Ne to Fe line ratios of TW Hya are somewhat more extreme than, but not dissimilar to, those of e.g. II Peg and UX Ari. This similarity — and, in particular, the prominence of lines of highly ionized Ne — could suggest that at least some of the X-ray emission from TW Hya originates in strong flares during which material is evaporated from the stellar photosphere. Evidence for such time-dependent abundance anomalies has been noted for certain late-type stars (e.g., Tsuboi et al. 1998; Brinkman et al. 2001; Audard et al. 2001; see also discussion in Feigelson 2001). In the present case, however, there is no evidence that (for example) the overabundance of Ne is more pronounced while TW Hya is in a flaring state.

The flare observed during our observation of TW Hya displayed very different behavior from flares seen on RS CVn stars. For example, Huenemoerder et al. (2001) report a flare on II Peg that rose more slowly and decayed exponentially, consistently with Solar 2-ribbon flares (an arcade of loops undergoing continuous reconnection). In contrast, the flare observed on TW Hya displayed a sharp rise and nearly linear decay. Kastner et al. (1999) observed flares of similar magnitudes and rise and decay times with ASCA and noted that the pointed and all-sky survey ROSAT Position Sensitive Proportional Counter count rates for TW Hya differ by a factor of two, suggesting that TW Hya routinely flares in this manner.

More importantly, there are significant differences between the spectra of TW Hya

and all active, late-type stars thus far observed with Chandra/HETGS, particularly in the ratios within the density-sensitive triplet line complexes of He-like ions (Fig. 6). The large electron densities implied by the O VII and Ne IX triplets,  $\log n_e > 12$  (cgs), are 2-3 orders of magnitude higher than those inferred from Chandra/HETGS spectra obtained thus far for active, late-type (RS CVn) stars (Canizares et al. 2000; Huenemoerder et al. 2001). It is a long-standing paradigm that activity in such stars is due to Solar-like activity scaled up by faster rotation and the consequent stronger magnetic dynamo (and not, for instance, close-binary interaction, except via tidally induced rotation). TW Hya has, in contrast, a higher density and somewhat cooler X-ray emitting region than these “traditional,” rotationally-driven dynamo sources.

It must be noted, however, that some stars have shown evidence of high coronal densities. From Fe XXI lines in EUVE spectra of  $\lambda$  And, Sanz-Forcada et al. (2001) found densities of 12.3 at  $\log T = 7$ , which increased to 12.9 during a flare. Brickhouse and Dupree (1998) reported a very high density, albeit with large uncertainties, of  $\sim 13$  for 44i Boo (HD 133640).

In the Sun, electron densities can be measured for a variety of coronal structures and temperatures. In a large flare Phillips et al. (1996a) measured  $\log n_e \approx 12$  (cgs) from Fe XXI lines formed near  $\log T = 7$ . Doschek et al. (1981) measured flare densities of  $\log n_e$  from 11–12 at the cooler temperatures of O VII. In long-duration, gradual (or two-ribbon) flares, Widing and Doyle (1990) found a logarithmic density of 10.3. In active regions, Phillips et al. (1996b) determined logarithmic densities of 9–11 from Fe XVII lines, while Kastner & Bhatia (2001) determined a logarithmic density of 10 from Fe XV lines.

In sum, a large range of densities is inferred in the Sun and other stars from high-resolution X-ray and EUV spectra. We do not expect a unique value in any case, since we are sampling emission which is differential in both temperature and density, and we will determine some mean value of density in the temperature range over which any particular diagnostic is sensitive. The important point here is the purely empirical result that at the temperatures of formation of O VII and Ne IX (6.3 and 6.6 dex, respectively), TW Hya displays much higher emitting region densities than those of coronally active stars.

#### 4.2. Evidence for and implications of accretion-powered X-ray emission

Given the preceding discussion and the evidence that TW Hya likely is surrounded by a circumstellar disk from which it is still accreting (e.g., Muzerolle et al. 2000), we consider the possibility that the X-ray emission originates not in coronal activity but in the accretion funnel(s) that connects the circumstellar disk to the star. The hypothesis that

the X-rays arise in accretion shocks along the funnel flows is supported by the emission measure distribution derived from DEM fitting (Fig. 5). The distribution is sharply peaked, in contrast to the broad distributions (spanning the range 2 MK to 20 MK) characteristic of quiescent X-ray emission from active, late-type stars (e.g., Huenemoerder et al. 2001, Drake et al. 2001). Furthermore the temperature characterizing the bulk of the plasma,  $\sim 3$  MK, is consistent with adiabatic shocks arising in gas at free-fall velocities of  $150 - 300 \text{ km s}^{-1}$  — the range imposed by measurements of the width of the  $\text{H}\alpha$  line ( $\sim 150 \text{ km s}^{-1}$ ; Muzerolle et al. 2000) and by the observation that the X-ray emission line profiles are unresolved by Chandra/HETGS. We further note that the volume of X-ray emitting plasma implied by the derived  $n_e$  and emission measure ( $\sim 1.5 \times 10^{53} \text{ cm}^{-3}$ ) is only of order  $10^{-6}$  of the volume of the star. This fractional volume is far smaller than typical of coronal X-ray sources (e.g., Huenemoerder et al. 2001) and appears more consistent with that of a “hot spot” (or spots) where accretion impacts the stellar surface.

If the X-ray emission emanates from such a region, then the densities inferred from He-like ions can be used to estimate the mass accretion rate, given estimates for the infall velocity ( $150\text{--}300 \text{ km s}^{-1}$ ) and filling factor of the accretion funnel at the surface of the star ( $\sim 5\%$ ; Costa et al. 2000). The inferred densities ( $\log n_e \approx 13$ ) then suggest that the mass accretion rate is  $\sim 10^{-8} M_\odot \text{ yr}^{-1}$ . Given the (considerable) uncertainties, this mass accretion rate is consistent with the rate suggested by the C IV  $\lambda 1549\text{\AA}$  line flux of TW Hya ( $1.2 \times 10^{-12} \text{ erg cm}^{-2} \text{ s}^{-1}$ ; Valenti et al. 2000), i.e.,  $\dot{M} \approx 3 - 6 \times 10^{-8} M_\odot \text{ yr}^{-1}$  (where this estimate is obtained from the method described in Johns-Krull et al. 2000). Both of these rates are more than an order of magnitude larger than the mass accretion rate deduced from  $\text{H}\alpha$  ( $\dot{M} \approx 4 \times 10^{-10} M_\odot \text{ yr}^{-1}$ ; Muzerolle et al. 2000).

While significant puzzles remain — most notably, the origin of the abundance anomalies observed in its X-ray spectrum — these results for TW Hya are consistent with the hypothesis that most or all of the X-ray luminosity of this star is derived from accretion rather than from coronal activity. Chandra/HETGS and XMM grating spectroscopy of well-studied, X-ray-luminous cTTS and wTTS in and near dark clouds, as well as of the many X-ray-bright wTTS in the TW Hya Association, would establish whether the physical conditions in the X-ray emitting region of TW Hya are representative of TTS and, thereby, might confirm or refute the notion that accretion contributes to the X-ray emission from cTTS. High-resolution X-ray spectra of wTTS will be of particular interest. If analysis of such spectra yields values of  $n_e$  and  $T_x$  similar to those found here for TW Hya, this would call into question the contention that all wTTS are diskless and/or are no longer accreting material from their disks.

The authors wish to thank Eric Feigelson, Andrea Dupree, and Steve Beckwith for



incisive comments and enlightening discussions. This research was supported in part by contracts SV-61010 and NA-39073 to MIT.

## REFERENCES

- Audard, M., Guedel, M., & Mewe, R. 2001, *A&A*, 365, L318
- Brickhouse, N. S. & Dupree, A. K. 1998, *ApJ*, 502, 918
- Brinkman, A.E., et al. 2001, *A&A*, 365, L324
- Canizares, C.R., et al. 2000, *ApJ*, 539, L41
- Costa, V. M., Lago, M. T. V. T., Norci, L., & Meurs, E. J. A. 2000, *A&A*, 354, 621
- Drake, J. et al. 2001, *ApJ*, 548, L81
- Doschek, G. A., Feldman, U., Landecker, P. B., & McKenzie, D. L. 1981, *ApJ*, 249, 372
- Feigelson, E.D. 2001, in “Magnetic Fields Across the Hertzsprung-Russell Diagram” (G. Mathys et al., eds), *ASP Conf. Ser.*, in press (astro-ph/0102326)
- Feigelson, E.D., & Montmerle, T. 1999, *ARAA*, 37, 363
- Houck, J.C., & DeNicola, L.A. 2000, in *Astronomical Data Analysis Software and Systems IX*, *ASP Conf. Ser.*, Vol. 216, p. 591
- Huenemoerder, D.P., Schulz, N.S., and Canizares, C.R., 2001, *ApJ*, 559 (in press)
- Johns-Krull, C. M., Valenti, J. A., & Linsky, J. L. 2000, *ApJ*, 539, 815
- Kastner, J.H., Huenemoerder, D.P., Schulz, N.S., & Weintraub, D.A. 1999, *ApJ*, 525, 837
- Kastner, J.H., Zuckerman, B., Weintraub, D.A., & Forveille, T. 1997, *Science*, 277, 67
- Kastner, S.O., & Bhatia, A.K. 2001, *ApJ*, 553, 421
- Krist J.E., Stapelfeldt K.R., Menard F., Padgett D.L., & Burrows C.J. 2000, *ApJ*, 538, 793
- Muzerolle, J., Calvet, N., Briceno, C., Hartmann, L., & Hillenbrand, L. 2000, *ApJ*, 535, L47
- Phillips, K. J. H., Bhatia, A. K., Mason, H. E., & Zarro, D. M. 1996a, *ApJ*, 466, 549
- Phillips, K. J. H., Greer, C. J., Bhatia, A. K., & Keenan, F. P. 1996b, *ApJ*, 469, L57
- Porquet, D. & Dubau, J. 2000, *A&AS*, 143, 495
- Sanz-Forcada, J., Brickhouse, N. S., & Dupree, A. K. 2001, *ApJ*, 554, 1079
- Shu, F.H., Shang, H., Glassgold, A.E., & Lee, T. 1997, *Science*, 277, 1475
- Skinner, S.L., Gudel, M., Koyama, K., & Yamauchi, S. 1997, *ApJ*, 486, 886

- Skinner, S.L., & Walter, F. M. 1998, *ApJ*, 509, 761
- Smith, R. K., Brickhouse, N. S., Liedahl, D. A., & Raymond, J. C. 2001, *ApJ*, 556, L91.
- Tsuboi, Y., Koyama, K., Murakami, H., Hayashi, M., Skinner, S., & Ueno, S. 1998, *ApJ*, 503, 894
- Trilling, D.E., Koerner, D.W., Barnes, J.W., Ftaclas, C., & Brown R.H. 2001, *ApJ*, 552, L151
- Valenti, J. A., Johns-Krull, C. M., & Linsky, J. L. 2000, *ApJS*, 129, 399
- Weintraub, D.A., Kastner, J.H., & Bary J.S. 2000, *ApJ*, 541, 767
- Wichmann, R., Bastian, U., Krautter, J., Jankovics I., & Rucinski, S.M. 1998, *MNRAS*, 301, L39
- Widing, K. G. & Doyle, J. G. 1990, *ApJ*, 352, 760
- Wilner D.J., Ho P.T.P., Kastner J.H., & Rodriguez L.F. 2000, *ApJ*, 534, L101
- White, N.E. 1996, in “Cool Stars, Stellar Systems, and the Sun”, Pallavicini, R. and Dupree, A.K. (eds.), *ASP Conf. Series*, 109, 193.

### Figure Captions

**Figure 1** ASCA SIS (CCD) spectrum (top) and Chandra/HETGS spectrum (bottom). The ASCA counts spectrum has bins of constant width in energy (29 eV). The Chandra/HETGS counts spectrum has 0.005Å bins and has been smoothed by a Gaussian with a width equal to the instrumental resolution ( $\sigma = 0.008\text{\AA}$ ).

**Figure 2** Selected regions of the medium energy grating (MEG) spectrum of TW Hya (solid curve). The observed spectrum is overlaid with a variable-abundance, differential emission measure model (dashed curve) that best fits temperature-sensitive line intensities (§3).

**Figure 3** Light curve obtained from the 48 ks Chandra/HETG observation of TW Hya, integrated over 1.7 Å to 25 Å for combined HEG and MEG orders -3 to +3 (excluding zero, which was not usable due to pileup). Bin sizes are 2 ks. The background is negligible.

**Figure 4** Measurements of the ratios of resonance ( $r$ ), intercombination ( $i$ ), and forbidden ( $f$ ) lines of Ne IX during the quiescent (Q) and flaring (F) states of TW Hya. Density- and temperature-sensitive diagnostics are represented by the ratios  $f/i$  and  $(f+i)/r$ , respectively. Dashed and dotted curves indicate contours of constant  $\log n_e$  and  $\log T$ , respectively. The results indicate that, despite an increase of a factor  $\sim 2$  in count rate at the onset of the flare, there was no measureable change in either  $n_e$  or  $T$  during the observation.

**Figure 5** Differential emission measure (DEM) as a function of temperature for TW Hya. This DEM is for the entire observation and thus represents a mean of flare and quiescent states. It was determined by fitting low-density limit model emissivities to the observed fluxes for many elements with their relative abundances as free parameters. The hatched region is an upper limit derived from flux upper limits on undetected high-ionization states of Fe.

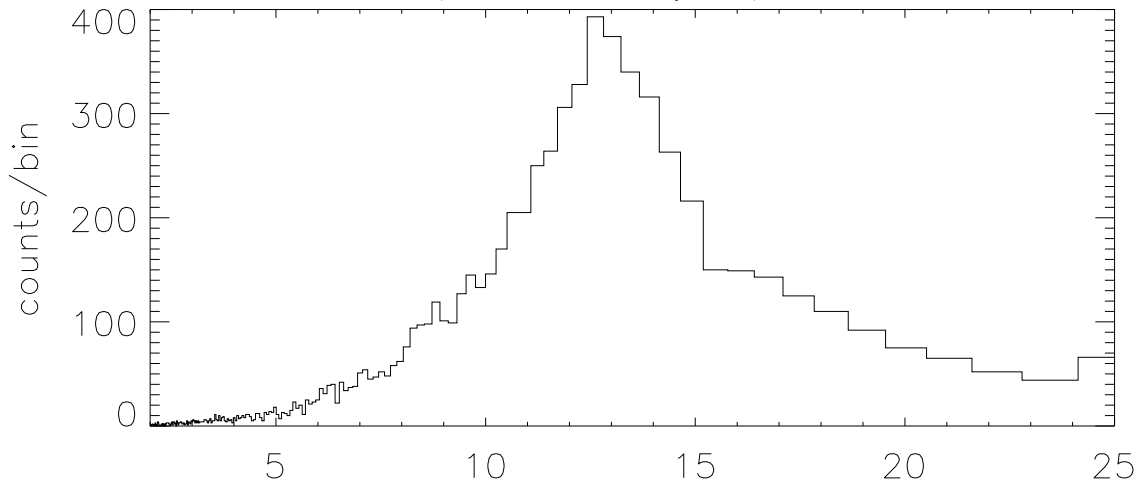
**Figure 6** Chandra/HETGS spectra of TW Hya and the active, late-type stars AB Dor (Chandra observation identifier [OID] 16), Capella (OID 1318), HR 1099 (OID 62538), AR Lac (OID 6, 9), TY Pyx (OID 601), UX Ari (OID 605),  $\lambda$  And (OID 609), and II Peg (OID 1451) in the spectral region encompassing the 13.56 Å He-like Ne IX triplet and the 15.01 Å Fe XVII line (see also Drake et al. 2001, Canizares et al. 2000, and Huenemoerder et al. 2001). Objects are RS CVn binaries (or similar systems) with the exception of TW Hya and the rapidly rotating K dwarf AB Dor. Spectra are shown as raw counts in the summed MEG  $\pm 1^{st}$  orders, in 0.005 Å bins, and have been smoothed

slightly. They are arranged from top to bottom roughly in order of the Ne IX 13.56 to Fe XVII 15.01 Å ratio, which is more sensitive to abundance than to temperature. Lines labeled are Ne IX, Fe XVII-XVIII, and O VII.

Table 1. TW Hydrae: Selected X-ray Emission Lines

Line	$\lambda_t^a$	$\lambda_o^b$	$f_l^c$	$\log T_{\max}^d$
Fe xxv	1.8504	1.8550 (0.0150)	(14.9) <sup>e</sup>	7.8
Si xiv	6.1805	6.1745 (0.0087)	2.7 (1.9)	7.2
Si xiii	6.6479	6.6480 (0.0080)	2.1 (1.7)	7.0
Si xiii	6.6882	6.6775 (0.0150)	0.8 (1.2)	7.0
Si xiii	6.7403	6.7400 (0.0052)	2.8 (1.7)	7.0
Fe xxiv	7.9857	7.9841 (0.0127)	1.4 (1.4)	7.3
Mg xii	8.4193	8.4157 (0.0062)	3.0 (2.0)	7.0
Ne x	9.7081	9.7000 (0.0150)	2.0 (2.1)	6.8
Ne x	10.239	10.2363 (0.0032)	7.8 (2.8)	6.8
Fe xxiv	10.619	10.6210 (0.0150)	(5.7) <sup>e</sup>	7.3
Fe xxiv	10.664	10.6788 (0.0150)	(5.3) <sup>e</sup>	7.3
Ne ix	11.544	11.5451 (0.0025)	18.0 (4.6)	6.6
Fe xxii-xxiii	11.737	11.7302 (0.0150)	(7.4) <sup>e</sup>	7.1
Ne x	12.132	12.1349 (0.0005)	73.7 (7.8)	6.8
Fe xvii	12.266	12.2700 (0.0100)	4.7 (4.0)	6.7
Fe xx	12.820	12.8164 (0.0150)	(13.1) <sup>e</sup>	7.0
Fe xx	12.835	12.8200 (0.0150)	(11.7) <sup>e</sup>	7.0
Ne ix	13.447	13.4508 (0.0008)	122.4 (11.9)	6.6
Ne ix	13.553	13.5547 (0.0008)	79.2 (10.5)	6.6
Ne ix	13.699	13.7004 (0.0027)	35.3 (8.6)	6.6
Fe xix	13.795	13.7898 (0.0150)	(8.4) <sup>e</sup>	6.9
Fe xvii	13.825	13.8223 (0.0150)	(10.0) <sup>e</sup>	6.7
Fe xviii	14.210	14.2109 (0.0124)	8.3 (6.9)	6.8
Fe xvii	15.014	15.0180 (0.0027)	(179.0) <sup>e</sup>	6.7
O viii	15.176	15.1791 (0.0150)	(15.9) <sup>e</sup>	6.7
Fe xvii	15.261	15.2605 (0.0026)	23.2 (8.4)	6.7
O viii	16.006	16.0107 (0.0025)	35.7 (10.4)	6.5
Fe xviii	16.073	16.0752 (0.0150)	(17.8) <sup>e</sup>	6.7
Fe xvii	16.780	16.7759 (0.0100)	15.3 (9.9)	6.7
Fe xvii	17.051	17.0511 (0.0048)	35.9 (13.1)	6.7
Fe xvii	17.096	17.0988 (0.0071)	25.4 (12.7)	6.7
O vii	18.627	18.6337 (0.0150)	10.8 (14.1)	6.3
O viii	18.967	18.9710 (0.0021)	195.7 (28.0)	6.5

ASCA/SIS X-ray Spectrum



Chandra/HETG X-ray Spectrum

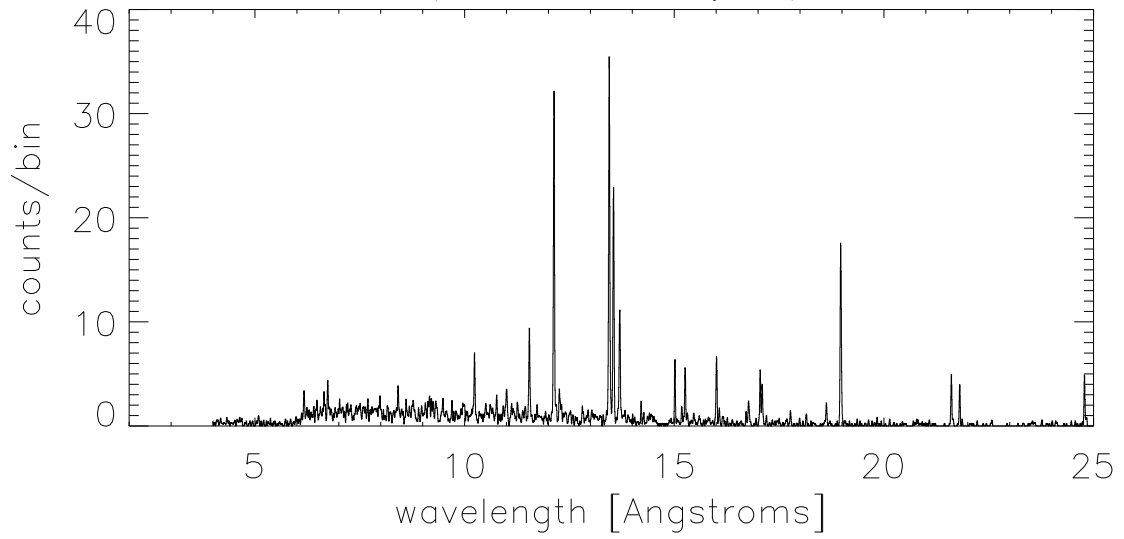


Table 1—Continued

Line	$\lambda_t^a$	$\lambda_o^b$	$f_l^c$	$\log T_{\max}^d$
O VII	21.602	21.6086 (0.0060)	91.3 (36.3)	6.3
O VII	21.804	21.8106 (0.0047)	105.4 (40.4)	6.3
O VII	22.098	22.1225 (0.0150)	(57.0) <sup>e</sup>	6.3
N VII	24.779	24.7859 (0.0050)	87.8 (36.5)	6.3

Note — The numbers in parentheses are values of standard deviation.

<sup>a</sup>Theoretical wavelengths of identification, in Å, from APED. If the line is a multiplet, we give the wavelength of the stronger component.

<sup>b</sup>Measured wavelength, in Å.

<sup>c</sup>Line flux is  $10^{-6}$  times the tabulated value in [phot cm<sup>-2</sup> s<sup>-1</sup>].

<sup>d</sup>Decimal logarithm of temperature [Kelvins] of maximum emissivity.

<sup>e</sup>Line flux is a  $2\sigma$  upper limit.

